Document downloaded from:

http://hdl.handle.net/10251/105878

This paper must be cited as:

Gonell-Gómez, F.; Boronat Zaragoza, M.; Corma Canós, A. (2017). Structure-reactivity relationship in isolated Zr sites present in Zr-zeolite and ZrO2 for the Meerwein-Ponndorf-Verley reaction. Catalysis Science & Technology. 7(13):2865-2873. doi:10.1039/c7cy00567a

The final publication is available at

https://doi.org/10.1039/c7cy00567a

Copyright The Royal Society of Chemistry

Additional Information

Journal Name

ARTICLE

Structure-reactivity relationship in isolated Zr sites present in Zr-zeolite and ZrO_2 for the Meerwein-Ponndorf-Verley reaction

Francisco Gonell, Mercedes Boronat,* Avelino Corma*

Received 00th January 20xx,
Accepted 00th January 20xx

DOI: 10.1039/x0xx00000x

www.rsc.org/

The influence of the crystallographic phase of ZrO_2 on its catalytic performance in the MPV reduction of cyclohexanone with propan-2-ol has been systematically investigated by combining accurate synthesis procedures, XRD and HRTEM characterization, kinetic measurements and DFT calculations, and compared to that of Zr-beta zeolite. The higher intrinsic activity of monoclinic zirconia as compared to other ZrO_2 phases is not due to a lower activation energy for the rate determining step, but to an adequate distribution of reactant fragments on the catalyst surface, indicating a structure-activity relationship for this reaction when catalyzed by ZrO_2 and also by Zr-beta zeolite. Unexpensive and stable ZrO_2 catalysts for the MPV reaction have been obtained by controlling the crystallographic phase of the synthesized material.

1. Introduction

The reduction of an aldehyde or a ketone via hydrogen transfer from an alcohol is called the Meerwein-Pondorf-Verley (MPV) reaction, and it is of particular interest because it is a very selective reaction, in which other reducible groups such as double bonds, carbon-halogen bonds and nitro groups are not reduced.[1] This reaction is known since 1925[2–4] and it has been classically catalyzed in homogeneous phase by aluminum or zirconium alkoxides, requiring an excess of the alkoxide between 100 and 200%.[5] The mechanism in homogeneous phase is well established, and involves coordination of both, ketone and deprotonated alcohol, to the metal center. Once coordinated, the reaction proceeds through a six-membered cyclic transition state where an hydride transfer takes place between the alcoholate and the ketone.[6] (Scheme 1)

The drawbacks associated to homogeneous non-recoverable catalysts in high excess have been overcome in the last years by the use of heterogeneous recyclable catalysts. In this sense, several solid catalysts have been successfully employed in this reaction, such as MgO,[7] ZrO_2,[5] grafted alkoxides,[8] and mesoporous materials.[9–18] Sn[9–12] and Zr-beta[13–17] zeolites, as well as Zr-MCM-41,[18] show very good activity in the MPV reduction. The tetrahedral metal coordination of the framework Zr^{4+} centers, which provides high Lewis acidity able to polarize the carbonyl group, is responsible of the high activity in this reaction.

The reaction mechanism over Sn and Zr-beta was theoretically investigated in our group and it was concluded that it consists of three steps: (1) alcohol adsorption and deprotonation, (2) ketone adsorption in the same metal center and hydride shift from alkoxide to ketone and (3) proton transfer from the catalyst to the alkoxide followed by alcohol desorption.[14] The rate determining step of the whole process is the hydride shift through a six-membered cyclic transition state equivalent to that proposed in homogeneous phase.

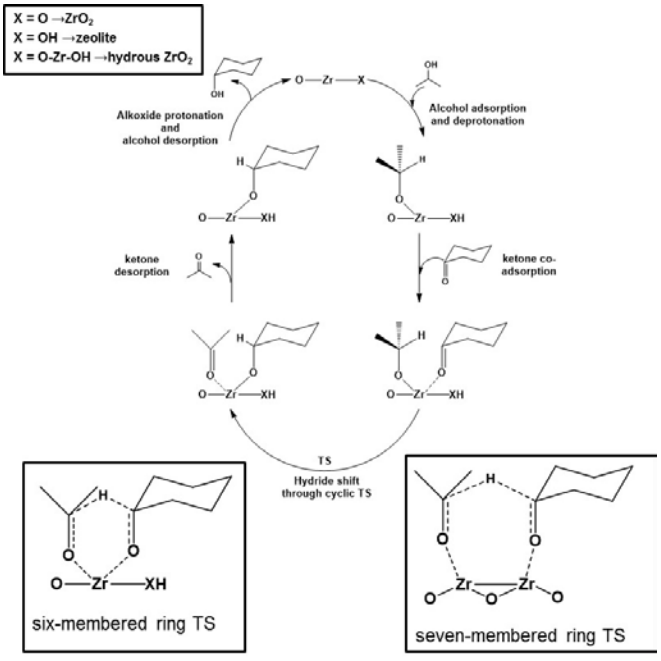

Scheme 1. General mechanism over ZrO_2, Zr-zeolites and hydrous ZrO_2 for the MPV reduction.

Zirconium oxide, which presents amphoteric character, high thermal and chemical stability, low costs and easy synthetic pathways,[19–21] is one of the most effective materials tested in the MPV reduction. It has been shown that both activity and selectivity depend on the synthetic procedure used, modifications in the catalyst acid-base properties, and on the concentration of surface hydroxyl groups.[22–

Instituto Tecnología Química, Universitat Politècnica de Valencia–Consejo Superior de Investigaciones Científicas, Av. de los Naranjos, s/n, 46022 Valencia, Spain

Please do not adjust margins

[24] In this sense, the amount of surface hydroxyl groups was tuned by annealing the hydrous zirconia at different temperatures, and it was observed that the higher the concentration of surface hydroxyl groups, the higher the activity of zirconia catalyst in the MPV reduction of cinnamaldehyde[8] and citral.[25] It was proposed that the hydroxyl groups act as sites for ligand exchange with alcohol to form the corresponding alkoxide on the catalyst, as also described for Sn- and Zr-beta zeolites.[14] This alkoxide will transfer the hydride to the aldehyde or ketone via the six-membered ring transition state classically proposed in the homogeneous mechanism (Scheme 1).

Very recently, Komanoya et. al.[20] reported that a mixture of tetragonal and monoclinic ZrO_2 is much more active than other oxides such as TiO_2 or Nb_2O_3. By means of an exhaustive spectroscopic study, they found that this zirconia mixture presents small amounts of Lewis acid sites with weak strength, and larger amounts of basic sites which are able to activate the methylene groups of the isopropoxide previously coordinated to a zirconium center, thus facilitating the formation of the cyclic transition state. The acid-base properties of zirconia polymorphs have been systematically studied by different authors, and it has been reported that monoclinic ZrO_2 presents stronger Zr^{4+} Lewis acid sites and stronger basic sites such as O^{2-} centres and Zr^{4+}-O^{2-} pairs.[26-28]

From the precedents commented above it appears that the crystallographic phase of zirconia could play a role in its catalytic performance, although no systematic study has been performed regarding the form (hydrous, monoclinic or tetragonal) of zirconia that is more active and selective in the MPV reduction. On the other hand, it is assumed that the mechanism of the MPV reduction over zirconium oxide is the same proposed for catalysts containing isolated Zr^{4+} species, (zirconium alkoxides in homogeneous phase and Zr-containing molecular sieves) but no experimental nor theoretical confirmation of this mechanism has been reported.

In this paper, different zirconia polymorphs have been synthesized through an accurate control of the synthetic parameters, and they have been tested in the MPV reduction of cyclohexanone with propan-2-ol. An intrinsically higher reactivity of monoclinic zirconia has been found which, according to a detailed kinetic study, is due to entropy effects associated to the correct distribution of the reactant molecules on the catalyst surface. The complete mechanism of the MPV reduction of cyclohexanone with propan-2-ol over monoclinic and tetragonal ZrO_2 surface models has been investigated using DFT methods, and a different pathway involving adsorption of the two reactant fragments on two different Zr centers is proposed for the first time. Combination of experimental and theoretical results provides new insights into the MPV reduction reaction mechanism over zirconium oxides, which allows a better understanding of the reaction and a more efficient catalyst design.

2. Experimental Section

2.1 Catalysts synthesis

2.1.1 Materials. $ZrO(NO_3)_2xH_2O$, $ZrOCl{\cdot}8H_2O$, urea, ammonia (25% volume), cyclohexanone, cyclohexanol, dodecane and propan-2-ol, were supplied by Sigma-Aldrich.

2.1.2 Synthesis. Pure monoclinic (*m*-ZrO_2-H sample) and tetragonal (*t*-ZrO_2-S sample) polymorphs were synthetized under hydrothermal conditions using urea as homogeneous precipitating agent. In this sense, in order to obtain the monoclinic polymorph the solvent used was water and for obtaining the tetragonal one methanol was chosen.[29] Briefly 0.6 mol of $ZrO(NO_3)_2xH_2O$ were dissolved in the 150 mL of the corresponding solvent, once dissolved 6 mol of urea were solubilized in the mixture and transferred to teflon-lined autoclave and heated to 150ºC for 18 h. The precipitated products were intensively washed and centrifuged in the mother solvent and dried at 100ºC overnight. Finally the materials were annealed at 400ºC in a muffle furnace in air atmosphere, with a temperature ramp rate of 5ºC/min and a dwell time of 2 h.

Two more materials were obtained through microwave-assisted synthesis.[30] 47 mmol of $ZrOCl_2{\cdot}8H_2O$ were dissolved in 80 mL of mili-Q water and this solution was transferred into two Teflon cups of 100 mL each and introduced in a microwave oven Synthos 3000 from Anton Paar. After sealing it, the temperature was increased at a heating rate of 20ºC/min until 220ºC, with a dwell time of 10 minutes. Then, the vials were allowed to cool to room temperature and the precipitates were washed and centrifuged several times. The material was dispersed in water and dialyzed until no chloride ions were detected. Finally, the suspension was dried under air flow. The material obtained by this procedure is pure monoclinic polymorph (*m*-ZrO_2-A sample). The same procedure was followed for obtaining a material composed by a mixture of 89% tetragonal and 11% monoclinic zirconia (*t*-ZrO_2-U sample) but in this synthesis 54 mmol of urea were dissolved in the zirconium precursor solution.

For hydrous zirconia (*hyd*-ZrO_2), 16.23 mmol of $ZrO(NO_3)_2{\cdot}xH_2O$ were dissolved in 500 mL of mQ water in a plastic vessel, after that the pH was increased to 11 using ammonia (25% volume) and left at this pH and at room temperature for 2 hours. The milky suspension was filtered and washed thoroughly with water and dried at 100ºC overnight.

2.2 Characterization techniques

XRD measurements were performed by means of a PANalytical Cubix'Pro diffractometer equipped with an X'Celerator detector and automatic divergence and reception slits using Cu-Kα radiation (0.154056 nm). The mean size of the ordered (crystalline) domains (*d*) was estimated using the Scherrer equation. The equation can be written as $d = \frac{0.9\,\lambda}{\beta\,cos\theta}$, where λ is the X-ray wavelength, β is the line broadening at half the maximum intensity (FWHM), after subtracting the instrumental line broadening, in radians, and θ is the Bragg angle. N_2 Adsorption–desorption isotherms were collected with a Micromeritics Gemini V gas adsorption analyzer at 77 K, after degassing the samples at 423 K overnight in a Micromeritics Flow prep 060 system with nitrogen flux gas. The BET surface areas were calculated from the adsorption branch of the isotherm according to the BJH method. Characterization by high-resolution transmission electron microscopy (HRTEM) was performed in a JEOL 2100F microscope operating at 200 kV.

2.3 Catalytic reactions

25 mg of the catalyst, 0.50 mmol cyclohexanone, 1 mL propan-2-ol and dodecane as standard were added to a reinforced glass reactor

 This journal is © The Royal Society of Chemistry 20xx

Please do not adjust margins

Please do not adjust margins

equipped with pressure controllers and the temperature was increased to the desired value with a silicon bath. During the experiment the reactors were stirred (magnetic stirring) at a rate of 1200 rpm. Samples were taken at different reaction times and analyzed by GC/MS and GC equipped with HP-5 column (30m×0.32×0.25µm) and a FID as detector, using dodecane as internal standard for the determination of conversion and yields.

2.4 Computational details

Periodic density functional theory (DFT) calculations were performed using the Perdew–Wang (PW91) exchange-correlation functional within the generalized gradient approach (GGA)[31,32] as implemented in the VASP code.[33] The valence density was expanded in a plane wave basis set with a kinetic energy cutoff of 450 eV, and the effect of the core electrons in the valence density was taken into account by means of the projected augmented wave (PAW) formalism.[34] All calculations are spin polarized. Integration in the reciprocal space was carried out at the Γ k-point of the Brillouin zone. Transition states were located using either the DIMER algorithm[35,36] or the nudged elastic band NEB method.[37,38]

The (ī11) facet of monoclinic zirconia and the (101) facet of tetragonal zirconia were represented by means of (2x2) and (2x3) supercell slabs, with dimensions 13.72 x 13.27 Å^2 and 12.85 x 11.09 Å^2, respectively. Both slab models contain 48 zirconium and 96 oxygen atoms arranged in three layers in the case of *m*-ZrO_2 and four layers in the case of *t*-ZrO_2, and with an empty region of ~20 Å between repeated slabs. During the geometry optimizations, the coordinates of the adsorbates and of the zirconium and oxygen atoms in the two uppermost layers of the ZrO_2 models were allowed to relax without any restriction until forces were below 0.02 eV Å^{-1}. Relative energies E_{rel} of adsorbed reactant, intermediate, transition state and product structures were calculated by substracting the total energy of the relaxed ZrO_2 model E(ZrO_2) and of optimized propan-2-ol E(C_3H_7OH) and cyclohexanone E($C_6H_{10}O$) from the total energy of the corresponding reactant, intermediate, transition state or product complex E(ZrO_2-complex), according to:

$$E_{rel} = E(ZrO_2\text{-complex}) - E(ZrO_2) - E(C_3H_7OH) - E(C_6H_{10}O)$$

Activation E_{act} and reaction ΔE energies were calculated as the difference between the total energy of the transition state TS or the product P for a given process and the corresponding reactant complex, according to the equations:

$$E_{act} = E(TS) - E(R)$$

$$\Delta E = E(P) - E(R)$$

3. Results and discussion

Different zirconia based materials were prepared following previously reported procedures.[29,30] Two zirconia samples with pure crystalline phase were synthesized hydrothermally (*m*-ZrO_2-H sample) and solvothermally (*t*-ZrO_2-S sample). Urea was used in both synthesis as homogeneous precipitating agent, and the only difference was the solvent used, water and methanol for obtaining pure monoclinic *m*-ZrO_2-H and pure tetragonal *t*-ZrO_2-S polymorphs, respectively (Figure 1). Following a microwave-assisted route[30] we were able to obtain pure monoclinic zirconia (*m*-ZrO_2-A sample). By introducing urea in the reaction media, a sample containing 89% tetragonal and 11% monoclinic zirconia was also synthesized (*t*-ZrO_2-U sample). Finally, hydrous ZrO_2 (*hyd*-ZrO_2 sample) was synthetized by simple co-precipitation with ammonia. This material shows a broad band in the XRD pattern characteristic of its amorphous nature (Figure 1).

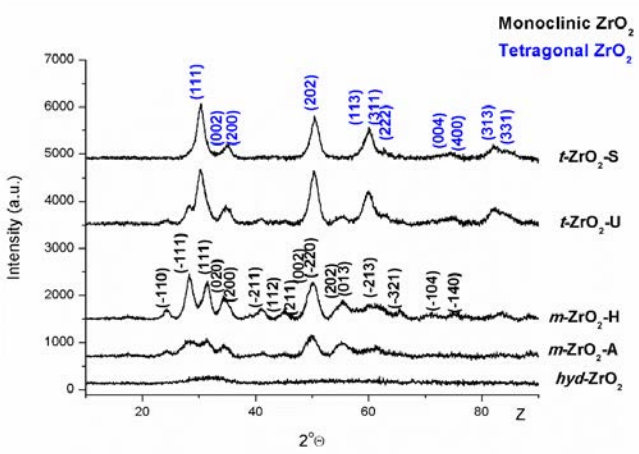

Figure 1. XRD pattern of *t*-ZrO_2-S, *t*-ZrO_2-U, *m*-ZrO_2-H, *m*-ZrO_2-A and *hyd*-ZrO_2.

The crystal size of all samples was calculated from the XRD data using the Scherrer equation (see Table 1). A particle size around 5 nm was determined for *m*-ZrO_2-H, *t*-ZrO_2-S and *t*-ZrO_2-U samples, and as a consequence the surface area of these three materials was found to be similar, in the 120 – 150 m^2 g^{-1} range. Special attention requires the *m*-ZrO_2-A sample, which shows a very small crystal size (2.5 nm) and therefore high surface area (220 m^2/g). On the other side, *hyd*-ZrO_2 has the largest surface area of all materials synthesized. The number of surface Zr sites in each sample was estimated assuming a surface density of 1.6842 10^{-5} moles of Zr atoms per m^2 for monoclinic zirconia and 1.3987 10^{-5} moles of Zr atoms per m^2 for the tetragonal polymorph, which were obtained from the periodic slab models of the extended (ī11) and (101) surfaces used in the DFT study. In the case of *hyd*-ZrO_2 the number of surface Zr sites was estimated assuming that it shows tetragonal structure, since previous works showed that the amorphous zirconia presents, at short range, a very similar structure to tetragonal ZrO_2.[39]

Table 1. Crystal size calculated by the Scherrer equation, BET surface area, and number of surface Zr sites for different ZrO_2 samples.

Sample	Crystal Size (nm)	BET area (m^2·g^{-1})	Surface Zr sites × 10^3 (mol g^{-1}))
m-ZrO_2-A	2.5	210.0	3.54
t-ZrO_2-U	4.9	136.6	1.95
m-ZrO_2-H	5.0	152.1	2.56
t-ZrO_2-S	5.3	120.7	1.69
hyd-ZrO_2	-	297.0	4.15

Please do not adjust margins

Please do not adjust margins

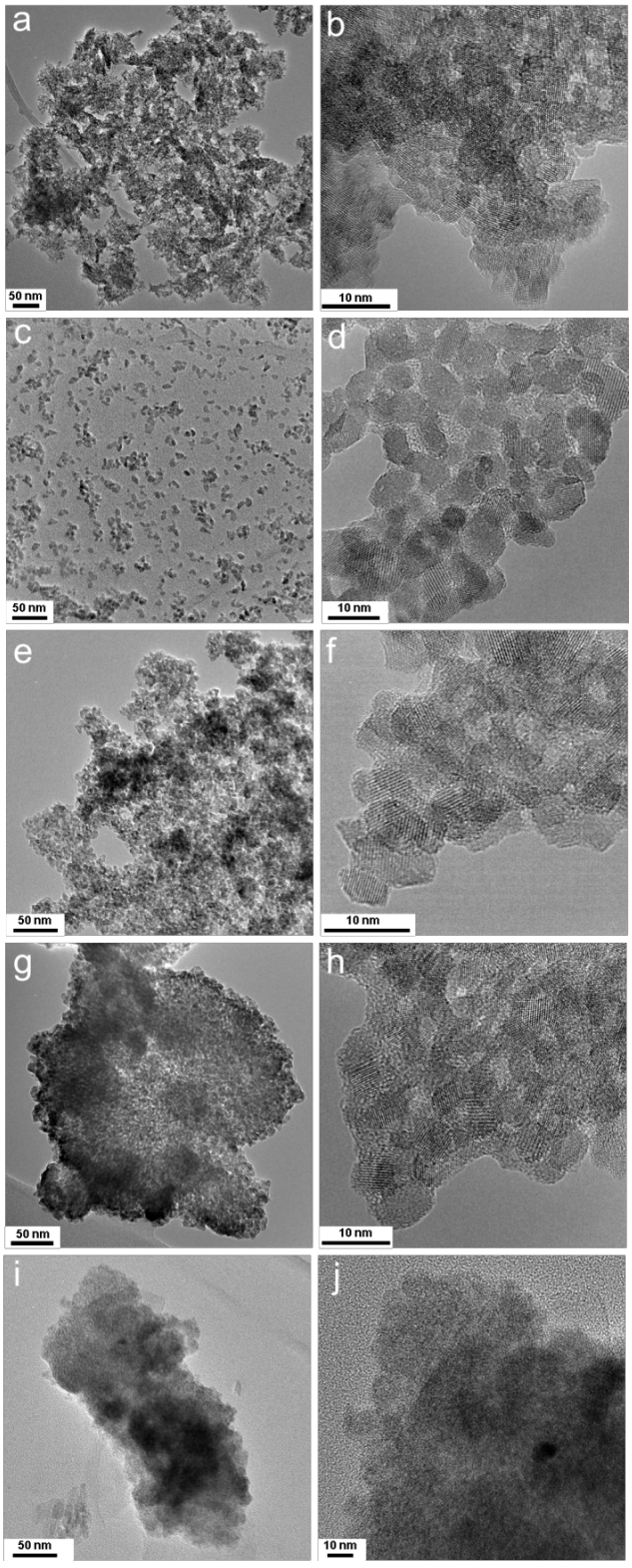

Figure 2. HRTEM micrographs of *m*-ZrO_2-A (a and b), *t*-ZrO_2-U (c and d), *m*-ZrO_2-H (e and f), *t*-ZrO_2-S (g and h) and *hyd*-ZrO_2 (i and j).

The HRTEM micrographs (Figure 2) show that *m*-ZrO_2-A is composed of nanoparticles with a diameter of ~ 3 nm while a particle size around 5 nm is determined for *t*-ZrO_2-U, *m*-ZrO_2-H and *t*-ZrO_2-S, in good agreement with the crystal sizes calculated form the XRD data. All these four materials show high crystallinity thus the lattice crystals are clearly visible when the magnification is increased (Figure 2 b, d, f and h). On the other hand for *hyd*-ZrO_2 no lattice crystals are visible as consequence of its amorphous nature (Figure 2 j).

The five materials were tested in the MPV reduction of cyclohexanone to cyclohexanol using propan-2-ol as solvent, and the yields of product as a function of time are compared in Figure 3. The two monoclinic zirconias are quite active in the MPV reduction, with the cyclohexanol yield obtained for *m*-ZrO_2-A and *m*-ZrO_2-H being 91 and 85 %, respectively, at three hours of reaction time. As the content of tetragonal polymorph increases the activity decreases, thus *t*-ZrO_2-U (with 89% vol. *t*-ZrO_2) and *t*-ZrO_2-S (100% vol. *t*-ZrO_2) show 32 and 7 % cyclohexanol yield, respectively, at three hours of reaction time. Finally, hydrous zirconia shows an intermediate activity, with 42% cyclohexanol yield at the same reaction time.

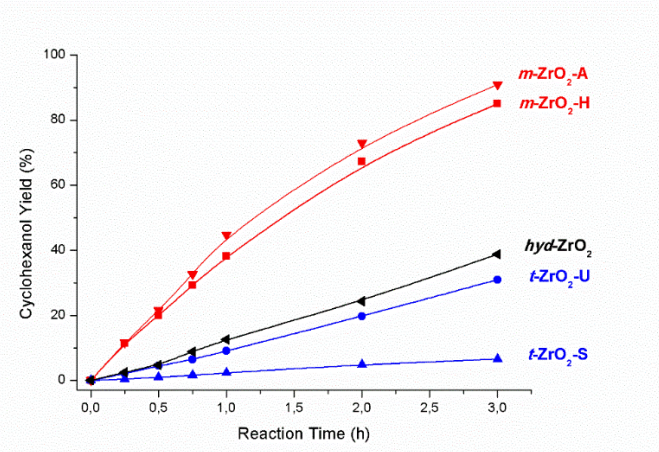

Figure 3. MPV reduction of cyclohexanone with propan-2-ol catalyzed by zirconia. Yield of cyclohexanol as a function of time for m-ZrO_2-A (red triangles), m-ZrO_2-H (red squares), t-ZrO_2-U (blue circles), t-ZrO_2-S (blue triangles) and hyd-ZrO_2 (black triangles) samples. Reaction conditions: 0.5 mmol cyclohexanone, 1 mL propan-2-ol, dodecane as standard, 25mg catalyst, 80°C.

For a more accurate comparison of samples having different surface area and therefore different number of accessible Zr active sites, turnover frequencies (TOF) were calculated from initial reaction rates (r_0) measured at 15 min reaction time (Table 2). The initial reaction rates over the monoclinic zirconia samples are ~ 5 times faster than over hydrous zirconia, and almost 30 times faster than over the pure tetragonal *t*-ZrO_2-S sample. When the number of surface Zr sites is taken into account by calculation of TOF, it becomes evident that monoclinic zirconia is intrinsically more reactive than tetragonal or amorphous polymorphs, with the *m*-ZrO_2-H sample being the most active. For comparison, the same tests were carried out using a Zr-beta zeolite sample with a Si/Zr ratio = 149. In order to have measurable initial rates, the amount of catalyst had to be decreased to 10 mg at the same reagents concentration, which indicates that Zr-beta is much more active than the other zirconia polymorphs. Indeed, the TOF calculated for Zr-beta is considerably larger than those for ZrO_2 samples (Table 2).

This journal is © The Royal Society of Chemistry 20xx

Please do not adjust margins

Please do not adjust margins

Table 2. Catalytic activity and kinetic parameters calculated for different ZrO_2 samples and Zr-beta zeolite.

Sample	$r_0 \times 10^3$ (mol h^{-1} g^{-1})	TOF (h^{-1})	E_{act} (kJ·mol^{-1})
m-ZrO_2-A	9.36	2.64	45.2
t-ZrO_2-U	2.00	1.03	42.7
m-ZrO_2-H	9.12	3.56	48.1
t-ZrO_2-S	0.32	0.19	45.0
hyd-ZrO_2	1.68	0.40	51.9
Zr-beta	12.55	113.11	40.9

The higher activity of monoclinic zirconia as compared to the other ZrO_2 polymorphs could be initially related to the presence of stronger Lewis acid and basic sites in this material,[26-28] although this argument alone might not explain the excellent performance of Zr-beta zeolite. Going one step further, the kinetics of the reaction were investigated over the five materials characterized above and over Zr-beta zeolite. Assuming that the rate determining step is the H shift between propoxide and cyclohexanone, the initial reaction rate can be described by $r_0 = k_{HS}$ [propoxide][cyclohexanone]. As propan-2-ol is in high excess, the reaction can be considered as a pseudo-first order reaction, with r_0 only depending on the concentration of cyclohexanone, $r_0 = k\cdot$[cyclohexanone], where $k = k_{HS}$[propoxide]. By plotting the initial reaction rate versus the initial concentration of cyclohexanone at different temperatures straight lines were obtained, and from the slope of the fitted equations the kinetic constant *k* was deduced. The apparent activation energies E_{act} were calculated from the measured initial rates at different temperatures according to equations 1 and 2, where *A* is the frequency factor and *R* is the gas constant.

$$k = Ae^{\frac{-E_{act}}{RT}} \quad (1)$$

$$lnk = lnA - \frac{E_{act}}{R}\left(\frac{1}{T}\right) \quad (2)$$

Figure 4 shows the Arrhenius plots for the six catalysts studied, in which no appreciable difference in the calculated apparent activation energies is observed (see also E_{act} values in Table 2).

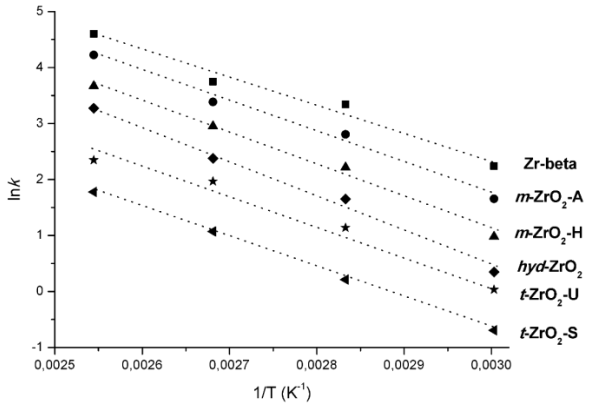

Figure 4. Arrhenius plots for MPV reduction of cyclohexanone with propan-2-ol.

Despite the significantly higher intrinsic activity of Zr-beta zeolite, the apparent activation energy calculated for this catalyst is 40.9 kJ/mol, which is in the same range as the other materials (Figure 4), and also quite similar to those reported for ZrO_2, TiO_2 and Nb_2O_3.[20] In contrast to the similar activation energies obtained for all catalysts tested, very different values were calculated for the pre-exponential frequency factor *A* obtained from the intersection with the ordinate of the Arrhenius plots in Figure 4. This frequency factor is related to the fraction of molecules that collide in the correct orientation to lead to the products. In the case of surface reactions with the reactants adsorbed on the catalyst, the frequency factor indicates the fraction of molecules that are adsorbed and activated in a suitable way. From these results it can be concluded that the great difference in the catalytic activity of zirconia polymorphs cannot be attributed to different activation energies, but it is consequence of the difference in the frequency factor *A*, associated to the correct orientation of reactant molecules on the catalyst surface.

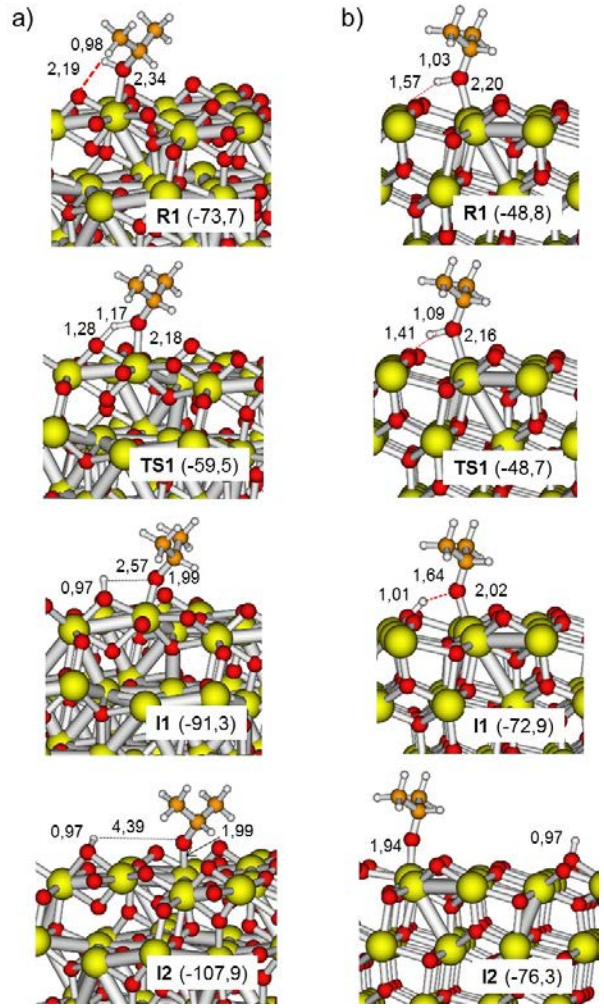

Figure 5. Optimized geometry of reactant R1, transition state TS1 and intermediate I1 and I2 structures involved in the deprotonation of propan-2-ol over a) *m*-ZrO_2 and b) *t*-ZrO_2. Distances in Å. Relative energies E_{rel} with respect to isolated ZrO_2 surface and propan-2-ol in kJ/mol are given in parenthesis. Zr, O, C and H atoms are depicted in yellow, red, orange and white, respectively.

This journal is © The Royal Society of Chemistry 20xx

Please do not adjust margins

Please do not adjust margins

To explain these observations, the mechanism of the MPV reduction of cyclohexanone with propan-2-ol over the most stable crystallographic facet of *m*-ZrO_2 and *t*-ZrO_2 was theoretically investigated by means of DFT calculations, and compared with that previously reported for Zr-beta zeolite.[14] It should be noted that since the models and methods employed in both studies are not the same (cluster model with localized Gaussian basis sets in reference 14 versus a periodic approach with plane wave basis sets in the current study, as well as different functional and alcohol reactant molecule) a straightforward comparison of the calculated values is not possible, and only mechanistic trends can be discussed.

As described before, the mechanism involves three main steps depicted in Scheme 1: propan-2-nol deprotonation yielding an adsorbed propoxide intermediate, cyclohexanone co-adsorption and hydride shift from propoxide to cyclohexanone through a cyclic transition state, and final protonation and desorption of cyclohexanol. The optimized geometries of the structures involved in the first elementary step on *m*-ZrO_2 and *t*-ZrO_2 surface models are depicted in Figure 5, together with the relative energy E_{rel} of each structure with respect to separated ZrO_2 surface model and reactant molecules. Formation of the adsorption complex R1 is more exothermic on *m*-ZrO_2 than on *t*-ZrO_2, and involves on one hand interaction of the O atom of the alcohol hydroxyl group with the Zr Lewis acid center, and on the other hand formation of a hydrogen bond between the alcoholic proton and a basic surface O atom. The higher stability of the R1 complex in *m*-ZrO_2 is in agreement with the previously reported relative strength of Lewis acid and basic sites in monoclinic and tetragonal ZrO_2 polymorphs.[26-28] In a similar way, cyclohexanone adsorption is considerably more exothermic on *m*-ZrO_2 (-74.3 kJ/mol) than on *t*-ZrO_2 (-27.4 kJ/mol) confirming the presence of stronger Zr^{4+} Lewis acid sites in the monoclinic polymorph.

Alcohol deprotonation occurs through transition state TS1 structure yielding a surface propoxide intermediate I1 that shifts to a more stable position on the catalyst surface, intermediate species I2. The process is the same on the two ZrO_2 models considered, but the energies involved are not completely equivalent. Deprotonation of propan-2-ol on *m*-ZrO_2 involves an activation energy of 14.2 kJ/mol, and the second intermediate structure I2 with the propoxide fragment distant from the proton is 16.6 kJ/mol more stable than intermediate I1. In contrast, the activation barrier necessary to deprotonate propan-2-ol on *t*-ZrO_2 is almost negligible, and the relative stability of the two intermediates I1 and I2 is quite similar. As will be shown later, this fact has important implications on the reactivity of t-ZrO_2.

The second step in the mechanism is co-adsorption of cyclohexanone close to the propoxide species, and hydride transfer between the two fragments. The optimized geometries and relative energies of the species involved in this elementary step are shown in Figure 6. The first important results is that, differently to the mechanisms reported for homogenous Zr-alkoxides and for Zr-containing zeolites, in the case of zirconium oxide the two reactant fragments (cylohexanone and propoxide) do not adsorb on the same Zr center but on two close surface Zr atoms separated by an O atom (see structures labeled R2 in Figure 6). In this situation, the distance between the H atom of the propoxide fragment that is going to shift and the C atom of the C=O group in cyclohexanone at which it will finally be attached is larger than 3 Å. The hydride shift occurs in this case through a seven-membered ring transition state (TS2 in Figure 6) in which the transferring H atom is at around 1.3 – 1.4 Å from the two C atoms involved in the process. Finally, in intermediate I3, propanone and a cyclohexoxide fragment have been formed.

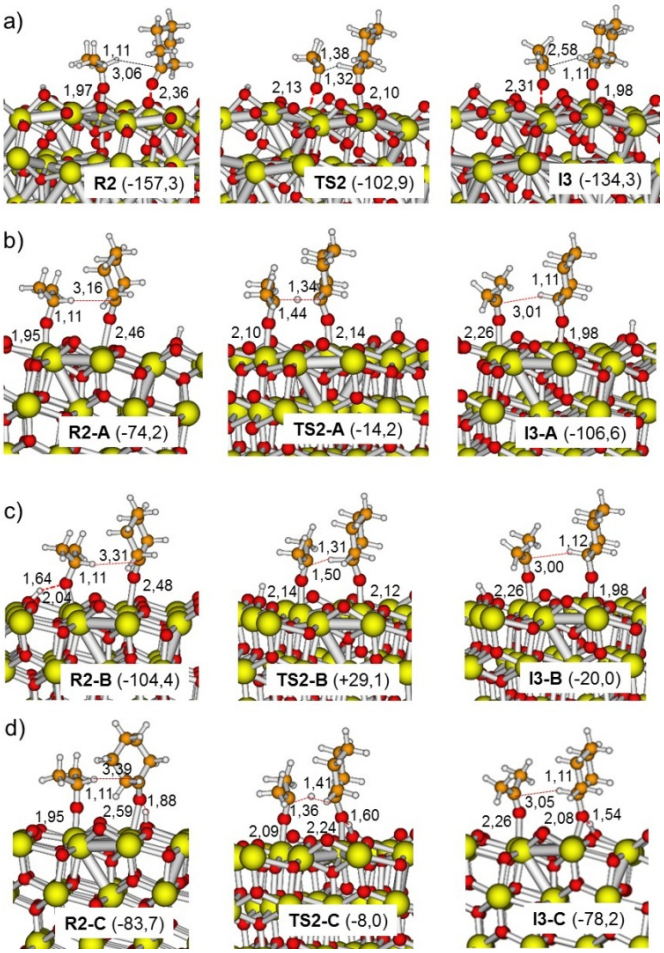

Figure 6. Optimized geometry of reactant R2, transition state TS2 and intermediate I3 structures involved in the hydride shift step over a) *m*-ZrO_2, b) *t*-ZrO_2 route A, c) *t*-ZrO_2 route B and d) *t*- ZrO_2 route C. Distances in Å. Relative energies E_{rel} with respect to isolated ZrO_2 surface, propan-2-ol and cyclohexanone in kJ/mol are given in parenthesis. Zr, O, C and H atoms are depicted in yellow, red, orange and white, respectively.

As for propan-2-ol deprotonation, the energies calculated on *m*-ZrO_2 and on *t*-ZrO_2 are quite different. Co-adsorption of cyclohexanone in structure I2 forming R2 on *m*-ZrO_2 is exothermic by 49.4 kJ/mol, the activation energy for the hydride shift is 54.4 kJ/mol, and the process is endothermic by 23.0 kJ/mol (Figure 6a). In contrast, co-adsorption of cyclohexanone on system I2 forming R2-A on *t*-ZrO_2 (Figure 6b) is nearly thermoneutral, the activation energy barrier for the hydride shift is slightly larger, 60 kJ/mol, and the process is clearly exothermic, releasing 32.4 kJ/mol. The different energy values obtained for co-adsorption of cyclohexanone on I2 in *m*-ZrO_2 and *t*-ZrO_2 models reflect again the stronger Lewis acidity of Zr^{4+} sites in *m*-ZrO_2. But the most relevant finding is that co-adsorption of

This journal is © The Royal Society of Chemistry 20xx

Please do not adjust margins

Please do not adjust margins

cyclohexanone on the intermediate structure I1 on *t*-ZrO_2 (Figure 6c) is exothermic by 31.5 kJ/mol, and yields a highly stable reactant structure R2-B in which the propoxide fragment is still stabilized by a hydrogen bond with the proton generated in the first deprotonation step. From this structure, the activation energy necessary for the hydride shift through TS2-B is as high as 133.5 kJ/mol and the process is endothermic by 84.4 kJ/mol. Even a third pathway was obtained on *t*-ZrO_2 (Figure 6c) in which the proton generated in the first deprotonation step interacts with co-adsorbed cyclohexanone in reactant structure R2-C. The energy released by cyclohexanone adsorption forming this complex is intermediate between the two previously discussed, 7.4 kJ/mol, the activation energy starting from this reactant complex is 75.7 kJ/mol and the process is slightly endothermic. This means that although a pathway exists on *t*-ZrO_2 involving an activation barrier of 60 kJ/mol, which is comparable to that calculated on *m*-ZrO_2 and to the values obtained experimentally, the reactant structure from which this pathway starts is significantly less stable than other arrangements of reactant fragments on the catalyst surface that lead to too high activation barriers and therefore to a lesser reactivity.

Thus, the different frequency factors *A* obtained from the kinetic studies on *m*-ZrO_2 and *t*-ZrO_2 are associated to a different distribution of reactant fragments on both surfaces. The most stable arrangement of reactant fragments on *m*-ZrO_2 is the one leading to a hydride transfer step involving an activation energy of 54.4 kJ/mol, in agreement with experiment. In contrast, there are several distributions of reactant fragments on *t*-ZrO_2 leading to high activation energies for the hydride shift step, and the right arrangement involving an activation barrier of 60 kJ/mol, is not the most stable and therefore neither the most probable one.

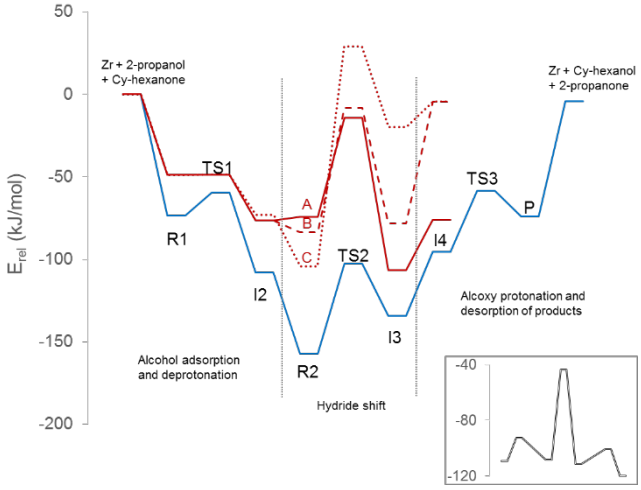

Figure 7. Calculated energy profiles for the MPV reaction over *m*-ZrO_2 (blue line), *t*-ZrO_2 (red lines) and Zr-beta zeolite (inset).

The last step in the mechanism is protonation of cyclohexoxide and desorption of the two products, propanone and cyclohexanol, from the catalyst surface. The calculated activation and reaction energies for this step over *m*-ZrO_2 are plotted in Figure 7, together with the complete energy profiles for the MPV reaction over *m*-ZrO_2 and *t*-ZrO_2 obtained in this work, and that previously reported for Zr-beta zeolite (inset). In this last case, the two fragments co-adsorb on the same isolated Zr^{4+} center, the hydride shift occurs through a six-membered transition state and the calculated activation energy for the rate determining step is 64.6 kJ/mol, in good agreement with the experimental value.

Despite the methodological differences between the present work on ZrO_2 polymorphs and the previous study on Zr-beta zeolite, we can still conclude that the significantly higher intrinsic reactivity of Zr-beta as compared to ZrO_2 polymorphs is due to its ability to bind the two reactant fragments to the same Zr^{4+} center, thus increasing the probability of hydride shift between them. On ZrO_2 however, a distribution of reactant fragments exists on the catalyst surface that considerably decreases the probability of finding cyclohexanone adsorbed close to a propoxide group. Moreover, while on *m*-ZrO_2 the most stable arrangement of the reactant fragments on the catalyst surface is structure R2, from which the hydride shift occurs with an activation energy barrier of 54.4 kJ/mol, on *t*-ZrO_2, the proper distribution of reactant fragments on the oxide surface leading to an activation energy of 60 kJ/mol for the hydride shift step (pathway A, solid red line) is not the most stable one, and other distributions involving too high activation energies (133.5 and 75.7 kJ/mol for pathways B and C, respectively) compete with this one. This explains the lower reactivity of *t*-ZrO_2 associated not to a higher activation energy but to a lower probability of finding the reactant molecules adsorbed in the proper way.

4. Conclusion

The influence of the crystallographic phase of zirconia on its catalytic performance in the MPV reduction of cyclohexanone with propan-2-ol has been systematically investigated by comparing the activity of five different samples including hydrous, monoclinic and tetragonal polymorphs. An intrinsically higher reactivity of monoclinic zirconia has been found which, according to a detailed kinetic study, is not due to a lower activation energy barrier on this polymorph, but to a most adequate distribution of the reactant molecules on the catalyst surface. The complete mechanism of the MPV reduction of cyclohexanone with propan-2-ol over the most stable crystallographic facet of *m*-ZrO_2 (ī11) and *t*-ZrO_2 (101) has been theoretically investigated using DFT methods. Differently to the mechanisms reported for catalysts containing isolated Zr^{4+} species that bind the two reactant fragments on the same site thus increasing the probability of H shift between them, the reaction pathway on zirconium oxide involves adsorption of the two reactant fragments on two close surface Zr atoms separated by an O atom. There exists therefore a distribution of reactant fragments on the catalyst surface that decreases the probability of finding them in the right arrangement and explains the significantly lower intrinsic reactivity of all ZrO_2 samples as compared to Zr-beta. On the other hand, the most stable arrangement of reactant fragments on *m*-ZrO_2 leads to an activation energy for the hydride transfer step in very good agreement with experiment, while on *t*-ZrO_2 there are several distributions of reactant fragments that compete with the right arrangement involving an accessible activation energy barrier, this being the reason of the lower reactivity of tetragonal zirconia samples as compared to monoclinic zirconia.

This journal is © The Royal Society of Chemistry 20xx

Please do not adjust margins

Please do not adjust margins

Acknowledgements

This work has been supported by the Spanish Government through "Severo Ochoa Program" (SEV 2012-0267). The Electron Microscopy Service of the UPV is acknowledged for their help in sample characterization. The Red Española de Supercomputación (RES) and Centre de Càlcul de la Universitat de València are gratefully acknowledged for computational facilities and technical assistance. F. Gonell is grateful to Ministerio de Educación, Cultura y Deporte for a PhD grant (AP2010-2748).

Notes and references

1 C. F. de Graauw, J. A. Peters, B. H. Van and H. J., *Synthesis,* 1994, **10**, 1007–1017.
2 A. Verley, *Bull. Soc. Chem. Fr.*, 1925, **37**, 537.
3 H. Meerwein and R. Schmidt, *Liebigs Ann. Chem.*, 1925, **444**, 221–238.
4 W. Ponndorf, *Angew. Chem.*, 1926, **39**, 138–143.
5 S. Makoto, K. Takahashi and H. Matsushita, *Bull. Chem. Soc. Jpn.*, 1988, **61**, 3283–3288.
6 R. Cohen, C. R. Graves, S. T. Nguyen, J. M. L. Martin and M. A. Ratner, *J. Am. Chem. Soc.*, 2004, **126**, 14796–14803.
7 A. M. Aramend, V. Borau, C. Jiménez, J. M. Marinas, J. R. Ruiz and F. J. Urbano, *Appl. Catal. A Gen.*, 2003, **244**, 207–215.
8 S. H. Liu, S. Jaenicke and G. K. Chuah, *J. Catal.*, 2002, **206**, 321–330.
9 A. Corma, M. E. Domine, L. Nemeth and S. Valencia, *J. Am. Chem. Soc.*, 2002, 3194–3195.
10 A. Corma, M. E Domine and S. Valencia, *J. Catal.*, 2003, **215**, 294–304.
11 M. Boronat, P. Concepción, A. Corma and M. Renz, *Catal. Today*, 2007, **121**, 39–44.
12 C. Paris, M. Moliner and A. Corma, *Green Chem.*, 2013, **15**, 2101–2109.
13 Y. Zhu, G. Chuah and S. Jaenicke, *J. Catal.*, 2004, **227**, 1–10.
14 M. Boronat, A. Corma and M. Renz, *J. Phys. Chem. B*, 2006, **110**, 21168–21174.
15 Y. Zhu, G. K. Chuah and S. Jaenicke, *J. Catal.*, 2006, **241**, 25–33.
16 M. Boronat, A. Corma, M. Renz and P. M. Viruela, *Chem. Eur. J.*, 2006, **12**, 7067–7077.
17 M. Koehle, R. Lobo, *Catal. Sci- Technol.*, 2016, **6**, 3018–3026.
18 V. L. Sushkevich, I. I. Ivanova, S. Tolborg and E. Taarning, *J. Catal.*, 2014, **316**, 121–129.
19 K. Tanabe and T. Yamaguchi, *Catal. Today*, 1994, **20**, 185–198.
20 T. Komanoya, K. Nakajima, M. Kitano and M. Hara, *J. Phys. Chem. C*, 2015, **119**, 26540–26546.
21 C. Battilocchio, J. M. Hawkins and S. V Ley, *Org. Lett.*, 2013, **15**, 2278–2281.
22 J. F. Miñambres, M. a. Aramendía, A. Marinas, J. M. Marinas and F. J. Urbano, *J. Mol. Catal. A Chem.*, 2011, **338**, 121–129.
23 F. J. Urbano, M. a. Aramendía, A. Marinas and J. M. Marinas, *J. Catal.*, 2009, **268**, 79–88.
24 J. F. Miñambres, A. Marinas, J. M. Marinas and F. J. Urbano, *Appl. Catal. B Environ.*, 2013, **140**–**141**, 386–395.
25 Y. Zhu, S. Liu, S. Jaenicke and G. Chuah, *Catal. Today*, 2004, **97**, 249–255.
26 W. Hertl, *Langmuir*, 1989, **5**, 96–100.
27 B. Bachiller-Baeza, I. Rodriguez-Ramos and A. Guerrero-Ruiz, *Langmuir*, 1998, **14**, 3556–3564.
28 K. Pokrovski, K. T. Jung and A. T. Bell, *Langmuir*, 2001, **17**, 4297–4303.
29 W. Li, H. Huang, H. Li, W. Zhang and H. Liu, *Langmuir*, 2008, **24**, 8358–66.
30 F. Gonell, D. Portehault, B. Julián-lópez, K. Vallé, C. Sanchez and A. Corma, *Catal. Sci. Technol.*, 2016, **6**, 8257–8267.
31 J. P. Perdew, J. A. Chevary, S. H. Vosko, K. A. Jackson, M. R. Pederson, D. J. Singh and C. Fiolhais, *Phys. Rev. B*, 1992, **46**, 6671.
32 J. P. Perdew and Y. Wang, *Phys. Rev. B*, 1992, **45**, 13244.
33 G. Kresse and J. Furthmüller, *Phys. Rev. B*, 1996, **54**, 11169.
34 P. E. Blöchl, *Phys. Rev. B*, 1994, **50**, 17953.
35 G. Henkelman and H. Jonsson, *J. Chem. Phys.*, 1999, **111**, 7010.
36 A. Heyden, A. T. Bell and F. J. Keil, *J. Chem. Phys.*, 2005, **123**, 224101.
37 G. Henkelman, B. P. Uberuaga and H. Jonsson, *J. Chem. Phys.*, 2000, **113**, 9901.
38 G. Henkelman and H. Jonsson, *J. Chem. Phys.*, 2000, **113**, 9978.
39 J. Livage, K. Doi and C. Mazières, *J. Am. Ceram. Soc.*, 1968, **51**, 349–353.

 This journal is © The Royal Society of Chemistry 20xx

Please do not adjust margins